Research Square

Preprints are preliminary reports that have not undergone peer review.
They should not be considered conclusive, used to inform clinical practice,
or referenced by the media as validated information.

Topology-dependent temporal memory in coupled oscillator networks

Yousef Jamali

Y.jamali@modares.ac.ir

Tarbiat Modares University

Article

Keywords: complex networks, synchronization, temporal memory, Kuramoto model, graph Laplacian, dynamical response

Posted Date: November 16th, 2026

DOI: https://doi.org/10.21203/rs.3.rs-11412580/v1

License: This work is licensed under a Creative Commons Attribution 4.0 International License.
Read Full License

Additional Declarations: No competing interests reported.

Topology-dependent temporal memory in coupled oscillator networks

Yousef Jamali*
Complex Systems Laboratory, Department of Applied Mathematics, School of Mathematical Sciences, Tarbiat Modares University, Tehran, Iran.
*Correspondence: y.jamali@modares.ac.ir

Abstract

Networks of interacting oscillators can move together to much the same degree while behaving very differently over time. This distinction matters because average synchronization alone may overlook how long coordinated activity persists along a network's connections. We investigated this hidden temporal memory using a noisy oscillator model and a measure comparing the instantaneous phase agreement of connected and unconnected node pairs. In 30 independent pairs of 128-node small-world networks, changing the connections while preserving every node's degree reduced the measure's correlation time from 2.178 to 1.159 time units, despite nearly identical average global synchronization (0.395 and 0.394). The difference remained, although smaller, after accounting for fluctuations in global synchronization. We then showed why network structure matters: a spectral description identifies the collective modes that contribute to memory and predicts their relaxation near synchronized states. Further simulations linked memory to dynamical modes in heterogeneous networks and demonstrated the importance of the sequence of interactions when synchronization is incomplete. These findings show that network architecture shapes not only how strongly a system coordinates, but also how long its coordination patterns persist. This perspective may inform studies of neural rhythms, engineered oscillator arrays and other interconnected systems.

Keywords: complex networks; synchronization; temporal memory; Kuramoto model; graph Laplacian; dynamical response.

Introduction

Synchronization gives a compelling language for describing how a crowd of individually oscillating units begins to move together. It appears in coupled physical oscillators, rhythmic biological circuits and networked technological systems [1, 2, 3, 4, 5]. In its simplest form, collective order is summarized by a single number: the coherence of the phases. That description is invaluable for determining whether a population acts in concert, yet two systems with similar average order may differ in *where* their coordination is concentrated and *how long* it persists. Such differences cannot be resolved by a time average alone.

The issue becomes especially interesting when the units interact through a complex network rather than all-to-all coupling. Sparse and heterogeneous graphs, small-world shortcuts and clustered neighborhoods provide distinct routes through which signals and dynamical perturbations propagate [6, 7, 8, 9, 10, 11]. Spectral and stability theories have clarified when coupling can support synchronization and how eigenmodes control relaxation [12, 13, 14, 15, 16, 17]. At the same time, the paths by which networks synchronize may differ markedly with topology, frequency organization and parameter regime [18, 19, 20, 21, 22]. A remaining practical question is therefore not only whether network structure

changes synchrony, but whether it changes the *temporal memory of a spatially structured observable* even when global synchrony is comparable.

This distinction has consequences beyond oscillator theory. In power-grid models, coordinated phase motion is necessary but does not by itself specify how network-level responses unfold after disturbances [23, 24, 25, 26]. In adaptive infrastructures or coevolving networks, the configuration of the links and the dynamics that traverse them can interact on different time scales [27, 28]. A measurement of temporal persistence could, in principle, complement ordinary coherence measures when assessing dynamical resilience or sensitivity. **We do not infer power-grid reliability or intervention performance from the simulations reported here**; those applications motivate the broader distinction between average coordination and its temporal organization.

The same conceptual problem also appears in neuroscience. The brain contains anatomically organized pathways but functional interactions fluctuate across space and time [29, 30, 31]. Cortical rhythms and coherence have long been linked to distributed neural communication [32, 33, 34]. Computational studies have demonstrated that anatomical connectivity, local oscillations, coupling and noise shape functional relationships at several temporal scales [35, 36, 37, 38]. Empirical studies likewise show that functional network organization is not stationary, but changes over time and cognitive state [39, 40, 41]. Importantly, event-based or edge-centric cofluctuation statistics can inherit structure from conventional correlation matrices, so a dynamic signature must be tested against relevant static and temporal alternatives [42, 43, 44]. Our observable is a phase-coherence contrast in synthetic oscillator networks, **not** a surrogate for measured blood-oxygen-level-dependent connectivity; its relevance here is methodological rather than a claim of clinical validity.

Two complementary lines of theory help organize the problem. Mean-field reductions can identify simple macroscopic behavior in appropriate oscillator ensembles [45, 46], whereas a graph-based spectral description resolves the modes along which collective configurations change. A recent spectral-transfer formulation has highlighted dynamical structure hidden below seemingly stationary global order [47]. Other studies have proposed local topological observables for detecting synchronization transitions or examined interactions between phase and amplitude coupling [48, 49]. Here the target is different: the persistence time of an explicitly edge-aligned phase observable under a topology-changing intervention, together with mechanisms that explain why this persistence changes.

Temporal memory also connects synchronization to stochastic dynamics and statistical mechanics. Linear stochastic systems translate relaxation rates into correlation times, but a single global time constant is generally insufficient when several dynamical modes contribute to an observable [50, 51, 52]. Response and spontaneous fluctuation are related under specific assumptions, including equilibrium reversibility, that need not hold in partially synchronized driven systems [53]. More generally, eliminating unresolved degrees of freedom induces effective memory and noise [54, 55, 56]. This history motivates a careful separation between (i) observable autocorrelation, (ii) fixed-point spectral approximation and (iii) tangent response along a time-dependent trajectory.

We therefore ask a direct question: **Can changing a network's wiring change the duration of edge-aligned fluctuations even when average global phase coherence remains nearly unchanged?** We address it through independent degree-preserving graph interventions, analytical modal identities, near-locking stochastic theory, and a separate time-dependent perturbation test. We also compare the mechanisms with contemporary approaches to modal and data-driven reduction [57, 58, 59, 60]. The aim

is not a general-purpose predictor of phase transitions, but a mechanistic account of a temporal property that a standard global synchronization summary does not determine.

Results

A rewiring intervention reveals memory hidden from average global coherence

For a simple undirected graph with structural edge set E and $m = |E|$ edges, we define the instantaneous edge–nonedge phase-coherence contrast

$$q(t) = \frac{1}{m} \sum_{(i,j)\in E} \cos\Big(\theta_i(t) - \theta_j(t)\Big) - \frac{1}{\bar{m}} \sum_{i<j,\,(i,j)\notin E} \cos\Big(\theta_i(t) - \theta_j(t)\Big),$$

where $\bar{m} = \binom{N}{2} - m$. Larger values mean that, at that instant, directly connected pairs are more phase-coherent on average than pairs without a direct structural link. The index is a contrast of phase similarity: it is *not* a Pearson correlation between structural and functional connectivity. We define its temporal memory τ_q as the first crossing of the centered, normalized autocorrelation $R_q(\tau)$ below e^{-1}; this crossing time should not be confused with an integral correlation time.

We generated 30 independent pairs of Watts–Strogatz graphs with $N = 128$ nodes. In each pair the second graph was produced by degree-preserving double-edge swaps, retaining the entire node-wise degree sequence and the same natural-frequency vector. The original coupling was fixed at $K = 1.90$; the rewired coupling was tuned using a **training-only** trajectory to match average global synchronization as closely as practical. Two new and independent noise sequences were then used to evaluate each pair, with these noise replicates averaged before graph-level inference. All graph and frequency seeds were distinct from the earlier exploratory series.

The mean Kuramoto order parameter r was 0.3952 in the original networks and 0.3940 after rewiring. Yet mean τ_q fell from 2.1782 to 1.1594 (Fig. 1), a reduction of approximately 47% relative to its original value. The mean paired difference was 1.0188 time units, with a graph-bootstrap 95% interval of 0.5412–1.7136. The original network had a longer memory in 27 of the 30 independent pairs (two-sided sign test $p = 8.43 \times 10^{-6}$). The temporal standard deviation of q likewise declined, from 0.0459 to 0.0203. This is an intervention-based effect on the *wiring*, not simply a relabeling of edges against an unchanged phase trajectory.

Could the difference be only a reflection of fluctuations in global coherence? Within each trajectory we regressed $q(t)$ on a nonlinear polynomial and short history of $r^2(t)$, then recomputed the first-crossing time of the residual. Memory still declined, from 1.1810 to 0.9016 time units; the paired difference was 0.2794 (95% graph-bootstrap interval 0.2141–0.3573; Fig. 1). The adjustment reduces a plausible common contribution but does not establish causal independence from the full trajectory of global order. Indeed, although mean r was matched, its temporal standard deviation was 0.1049 versus 0.0856. The empirical synchronization distributions are thus **not** identical. We restrict our inference to an approximately matched *mean* order parameter, rather than to two fully equivalent collective trajectories.

The original-versus-rewired difference was qualitatively robust to two numerical controls. In a sensitivity series on 12 graph pairs, moving the tuned rewired coupling by ± 0.08 did not eliminate the shorter memory of the rewired condition (Fig. 2). In a coupled-Brownian step-halving test on eight pairs, the direction persisted when dt was reduced from 0.05 to 0.025 (Supplementary Fig. S2). These checks

support the direction of the effect; they are not substitutes for a full convergence study or a fixed-coupling causal decomposition. Earlier tests on eight independent 256-node pairs supplied an additional, exploratory replication in the same direction.

The contrast admits an exact spectral representation

To understand what the order parameter misses, let L be the graph Laplacian, with eigenvectors u_a and eigenvalues λ_a, and set $z_i(t) = e^{\mathrm{i}\theta_i(t)}$ and $a_a(t) = u_a^{\top} z(t)$. The edge–nonedge contrast obeys the exact algebraic identity

$$q(t) = 1 + \frac{N+2m}{2\bar{m}} - \frac{N}{2\bar{m}}|a_1(t)|^2 - \left(\frac{1}{2m} + \frac{1}{2\bar{m}}\right)\sum_{a=2}^{N} \lambda_a |a_a(t)|^2.$$

For a connected graph, the first mode represents global phase coherence, since $|a_1|^2 = Nr^2$. The remaining terms quantify how activity is distributed across nontrivial structural modes. Thus a given global order parameter does not uniquely determine q, much less its memory. This identity holds for arbitrary phases, but it is not a closed evolution equation for the modal energies.

Near a fully phase-locked state with identical natural frequencies and sufficiently weak noise, transverse phase perturbations approximately follow independent Ornstein–Uhlenbeck modes. Their rates are $\gamma_a = K\lambda_a/\langle k \rangle$ and their stationary variances are $c_a = D/\gamma_a$. A second-order expansion of q gives the normalized autocorrelation

$$R_q(\tau) \simeq \frac{\sum_{a=2}^{N} b_a^2\, c_a^2 \exp(-2\gamma_a|\tau|)}{\sum_{a=2}^{N} b_a^2\, c_a^2}, \qquad b_a = \frac{1}{2}\left(\frac{N-\lambda_a}{\bar{m}} - \frac{\lambda_a}{m}\right).$$

Consequently, the memory of the contrast is a *weighted mixture* of modal relaxation times. A slow mode influences q only to the extent that the observable assigns it non-negligible weight. The smallest nonzero Laplacian eigenvalue, while important, is therefore not alone enough to predict the contrast's autocorrelation. In nonlinear near-locking simulations, the theory reproduced the ordering of memory times across small-world, rewired and random graph families (Fig. 3).

Heterogeneous phase locking exposes observable–mode overlap

The same idea can be extended beyond identical natural frequencies. At a stable heterogeneous locked solution, the Jacobian is proportional to a weighted Laplacian whose edge weights contain the cosine of the locked phase difference. Unlike the perfectly aligned state, the local expansion of q generally has **both linear and quadratic terms** in the fluctuations. The resulting covariance is a weighted sum of decays at rates γ_a and $\gamma_a + \gamma_b$. The weights now depend on the orientation of the observable's gradient and Hessian relative to the Jacobian eigenvectors—not simply on the unweighted graph spectrum.

Across 48 previously computed stable, heterogeneously locked networks, predicted and measured first-crossing times were strongly associated (Pearson $r = 0.975$), with mean absolute percentage error of approximately 7% (Fig. 4). This agreement links a concrete network-dependent observable to its local dynamical modes. It applies to fluctuations around stable locked solutions; drifting phases and partial synchronization require a different treatment.

Under partial synchrony, the order of interactions matters

In a partially synchronized network, the linearized generator $J(t)$ changes along the realized phase trajectory. Let $\Phi(t, t_0)$ be its time-ordered propagator. For a sufficiently small phase perturbation $\delta\theta(t_0)$ applied at time t_0, the first-order change of the contrast is

$$\delta q(t) \simeq \nabla q\big(\theta(t)\big)^{\top} \Phi(t, t_0)\, \delta\theta(t_0), \qquad \partial_t \Phi(t, t_0) = J(t)\Phi(t, t_0).$$

In the archived partially synchronized tests, kicked and reference trajectories were driven by the same noise. The tangent propagator using the actual Jacobian sequence reproduced their short-time difference accurately, whereas reversing or shuffling that sequence, or replacing it by its time average, increased reconstruction errors (Fig. 5). Temporal order can therefore matter strongly to response even when a conventional static descriptor remains similar. This perturbation result is **not** presented as a direct prediction of spontaneous autocorrelation: response–fluctuation equivalence needs additional assumptions that are not established here.

Discussion

Our findings reveal a simple but consequential distinction: a network's average level of synchronization does not fully describe how its coordinated activity unfolds over time. Two networks may appear almost identical when judged by a single global measure, yet differ markedly in how long phase relationships persist across their links. In our simulations, reorganizing connections while preserving the number of links at every node shortened this temporal memory. The result directs attention from how synchronized a network is to how its structure shapes the persistence of that synchronization.

The combination of controlled rewiring and mathematical analysis helps explain this difference. The rewiring experiments establish that changes in network organization accompany a reproducible change in memory, even when average synchronization is closely matched. Our exact spectral representation then shows how the measured contrast draws on several collective modes rather than only the global synchronization mode. Near strongly synchronized states, these modes relax at different rates, and the observed memory depends on how strongly each mode contributes. In heterogeneous phase-locked networks, theoretical predictions agreed closely with simulations. Together, these results provide a physical explanation for why similar average coordination can coexist with different temporal behavior.

When synchronization is only partial, the picture becomes more dynamic. The influence of one oscillator on another changes as their relative phases evolve. Consequently, the order in which these interactions occur affects the response to a small disturbance. Our time-dependent analysis captured this response much more accurately than a description based on average interactions. This finding complements the memory results: both emphasize the importance of the evolving network state, while spontaneous fluctuations and responses to imposed disturbances remain distinct quantities. A separate analysis of conditional responses and fluctuations is provided in the Supplementary Information.

The wider relevance of this distinction is that many interconnected systems are routinely summarized by a small number of average measures. In networks of power-grid oscillators or coordinated engineering devices, similar global phase alignment need not imply similar responses to disturbances. A measure of how long link-related coordination persists could add useful information to existing assessments of network behavior. In biological networks, including neural circuits, structural pathways constrain interactions while patterns of activity continually change. Our results offer a general modeling

perspective for asking how connectivity influences the duration of these patterns, without assuming that the present oscillator model directly represents any particular biological or technological system.

A strength of the approach is that it combines a measurable temporal quantity, a controlled change in connectivity, and mathematical predictions that can be checked independently. The degree-preserving intervention separates connection arrangement from the number of contacts per node, while the spectral treatment shows why the same global order can conceal different contributions from network modes. This framework suggests that the temporal signature of coordination is an informative network property in its own right, not merely an alternative way to display average synchrony.

The interpretation nevertheless has a defined scope. Coupling strength was adjusted after rewiring to match average synchronization, and the complete fluctuations of global synchronization were not identical between conditions. Rewiring also changes several structural properties at once. Accordingly, our results identify a robust topology-associated difference in memory, rather than isolating a single graph feature as its sole cause. The analytical approximations apply to specified synchronization regimes, and the partial-synchrony response analysis addresses small disturbances. These qualifications do not change the principal finding, but clarify what it establishes.

Future studies could vary clustering and spectral properties more independently and test the same ideas in models tailored to specific applications. The immediate conclusion is clear: understanding collective behavior requires attention not only to the strength of coordination, but also to its lifetime. Network wiring can shape both, and the relevant temporal effects can be traced to identifiable features of the system's dynamics.

Methods

Graph ensembles and oscillator dynamics

We studied undirected simple graphs with adjacency matrix A. Oscillator phases evolved according to the noisy, degree-normalized Kuramoto equation

$$d\theta_i = \left[\omega_i + \frac{K}{\langle k\rangle}\sum_{j=1}^{N} A_{ij}\sin\left(\theta_j - \theta_i\right)\right]dt + \sqrt{2D}\,dW_i.$$

Natural frequencies ω_i were sampled independently from a standard normal distribution and then held identical within each topology pair. The noise intensity was $D = 0.025$. The primary ensemble used Watts–Strogatz graphs with $N = 128$, initial degree $\langle k\rangle = 14$ and shortcut probability 0.2. Degree-preserving double-edge swaps were performed $5m$ times per original edge count; each graph and its counterpart had exactly the same degree sequence. The primary 30-pair series used fresh graph, frequency and rewiring seeds distinct from the exploratory datasets.

Design freeze, calibration and holdout evaluation

The original coupling was fixed to $K = 1.90$. Seven training-only bisection evaluations on $K \in [1.05, 2.60]$ calibrated the rewired graph against the original graph's training mean phase order. Training paths used 3,600 Euler–Maruyama steps, discarding 1,000. For testing, two independently generated noise paths per graph condition were simulated for 6,000 steps, discarding 1,800, with a sample saved every four steps. The numerical step was $dt = 0.05$. Common random numbers paired the noise across original and

rewired conditions within each holdout replicate; calibration noise was separate and never used to evaluate the primary endpoints. Parameters were frozen before the holdout trajectories were analyzed.

Observables and uncertainty

The global order parameter is $r(t) = \left|N^{-1}\sum_i e^{\mathrm{i}\theta_i(t)}\right|$. Edge and nonedge means in the definition of $q(t)$ were calculated by sparse-network identities checked against explicit pair sums on small graphs. For a centered scalar sequence x_t, the normalized sample autocorrelation at lag ℓ was calculated as

$$\hat{R}_x(\ell) = \frac{\sum_{t=1}^{T-\ell}(x_t - \bar{x})\,(x_{t+\ell} - \bar{x})}{\sum_{t=1}^{T}(x_t - \bar{x})^2}.$$

The first crossing below e^{-1} was interpolated linearly between samples. Within each trajectory, the synchronization-adjusted contrast was the least-squares residual from regression on an intercept, $r^2(t)$, $r^4(t)$, and the previous one and two recorded samples of r^2. This is a *descriptive adjustment*, not causal identification. Each independent graph–frequency pair, after averaging its two holdout replicates, was the independent unit of inference. Percentile intervals used 10,000 paired graph-level bootstrap draws. We report two-sided sign tests for directional replication and distinguish post-exploratory validation from preregistered confirmatory testing.

Numerical and theoretical controls

In 12 independently chosen pairs, the calibrated rewired coupling was changed by ± 0.08 in a sensitivity analysis using separate noise. Eight further pairs were reintegrated at $dt = 0.025$ and $dt = 0.05$ with coupled Brownian increments, preserving a comparable stochastic drive across discretizations. Exact spectral decomposition follows from $z^*Lz = \sum_{(i,j)\in E}\left|z_i - z_j\right|^2$ and the complete-pair coherence identity. The near-locking covariance formula follows from independent transverse Ornstein–Uhlenbeck modes and Gaussian fourth moments. The heterogeneous locked-state approximation uses the Jacobian's weighted Laplacian and a second-order Taylor expansion of the observable. For partial synchrony, a tangent propagator was integrated along the reference trajectory and evaluated against common-noise kicked controls. Detailed derivations, seeds and quality-control records are provided in the Supplementary Information and reproducibility archive.

Data availability

The study uses exclusively synthetic oscillator-network data. Graph-pair designs, pseudorandom seeds, model parameters, processed graph-level outcomes and primary validation data are included in the accompanying reproducibility archive. Data from supporting analyses are organized in the corresponding archived research stages.

Code availability

The Python code for the primary simulations, sensitivity analyses, numerical checks, and figure generation is included in the accompanying reproducibility archive. The README documents dependencies and commands for reproducing the reported analyses.

References

1. Acebrón, J. A., Bonilla, L. L., Pérez Vicente, C. J., Ritort, F. & Spigler, R. The Kuramoto model: a simple paradigm for synchronization phenomena. *Rev. Mod. Phys.* **77**, 137–185 (2005). https://doi.org/10.1103/RevModPhys.77.137.
2. Strogatz, S. H. From Kuramoto to Crawford: exploring the onset of synchronization in populations of coupled oscillators. *Physica D* **143**, 1–20 (2000). https://doi.org/10.1016/S0167-2789(00)00094-4.
3. Pikovsky, A., Rosenblum, M. & Kurths, J. *Synchronization: A Universal Concept in Nonlinear Sciences* (Cambridge Univ. Press, 2001).
4. Arenas, A., Díaz-Guilera, A., Kurths, J., Moreno, Y. & Zhou, C. Synchronization in complex networks. *Phys. Rep.* **469**, 93–153 (2008). https://doi.org/10.1016/j.physrep.2008.09.002.
5. Rodrigues, F. A., Peron, T. K. D. M., Ji, P. & Kurths, J. The Kuramoto model in complex networks. *Phys. Rep.* **610**, 1–98 (2016). https://doi.org/10.1016/j.physrep.2015.10.008.
6. Watts, D. J. & Strogatz, S. H. Collective dynamics of 'small-world' networks. *Nature* **393**, 440–442 (1998). https://doi.org/10.1038/30918.
7. Strogatz, S. H. Exploring complex networks. *Nature* **410**, 268–276 (2001). https://doi.org/10.1038/35065725.
8. Newman, M. E. J. The structure and function of complex networks. *SIAM Rev.* **45**, 167–256 (2003). https://doi.org/10.1137/S003614450342480.
9. Boccaletti, S., Latora, V., Moreno, Y., Chavez, M. & Hwang, D.-U. Complex networks: structure and dynamics. *Phys. Rep.* **424**, 175–308 (2006). https://doi.org/10.1016/j.physrep.2005.10.009.
10. Barabási, A.-L. & Albert, R. Emergence of scaling in random networks. *Science* **286**, 509–512 (1999). https://doi.org/10.1126/science.286.5439.509.
11. Newman, M. E. J. Assortative mixing in networks. *Phys. Rev. Lett.* **89**, 208701 (2002). https://doi.org/10.1103/PhysRevLett.89.208701.
12. Pecora, L. M. & Carroll, T. L. Master stability functions for synchronized coupled systems. *Phys. Rev. Lett.* **80**, 2109–2112 (1998). https://doi.org/10.1103/PhysRevLett.80.2109.
13. Barahona, M. & Pecora, L. M. Synchronization in small-world systems. *Phys. Rev. Lett.* **89**, 054101 (2002). https://doi.org/10.1103/PhysRevLett.89.054101.
14. Nishikawa, T., Motter, A. E., Lai, Y.-C. & Hoppensteadt, F. C. Heterogeneity in oscillator networks: are smaller worlds easier to synchronize? *Phys. Rev. Lett.* **91**, 014101 (2003). https://doi.org/10.1103/PhysRevLett.91.014101.
15. Donetti, L., Hurtado, P. I. & Muñoz, M. A. Entangled networks, synchronization, and optimal network topology. *Phys. Rev. Lett.* **95**, 188701 (2005). https://doi.org/10.1103/PhysRevLett.95.188701.
16. Restrepo, J. G., Ott, E. & Hunt, B. R. Onset of synchronization in large networks of coupled oscillators. *Phys. Rev. E* **71**, 036151 (2005). https://doi.org/10.1103/PhysRevE.71.036151.

17. Bayani, A. et al. The transition to synchronization of networked systems. *Nat. Commun.* **15**, 4955 (2024). https://doi.org/10.1038/s41467-024-48203-6.

18. Gómez-Gardeñes, J., Moreno, Y. & Arenas, A. Paths to synchronization on complex networks. *Phys. Rev. Lett.* **98**, 034101 (2007). https://doi.org/10.1103/PhysRevLett.98.034101.

19. Gómez-Gardeñes, J., Gómez, S., Arenas, A. & Moreno, Y. Explosive synchronization transitions in scale-free networks. *Phys. Rev. Lett.* **106**, 128701 (2011). https://doi.org/10.1103/PhysRevLett.106.128701.

20. Kalloniatis, A. C. From incoherence to synchronicity in the network Kuramoto model. *Phys. Rev. E* **82**, 066202 (2010). https://doi.org/10.1103/PhysRevE.82.066202.

21. McGraw, P. N. & Menzinger, M. Clustering and the synchronization of oscillator networks. *Phys. Rev. E* **72**, 015101(R) (2005). https://doi.org/10.1103/PhysRevE.72.015101.

22. McGraw, P. N. & Menzinger, M. Analysis of nonlinear synchronization dynamics of oscillator networks by Laplacian spectral methods. *Phys. Rev. E* **75**, 027104 (2007). https://doi.org/10.1103/PhysRevE.75.027104.

23. Dörfler, F., Chertkov, M. & Bullo, F. Synchronization in complex oscillator networks and smart grids. *Proc. Natl Acad. Sci. USA* **110**, 2005–2010 (2013). https://doi.org/10.1073/pnas.1212134110.

24. Rohden, M., Sorge, A., Timme, M. & Witthaut, D. Self-organized synchronization in decentralized power grids. *Phys. Rev. Lett.* **109**, 064101 (2012). https://doi.org/10.1103/PhysRevLett.109.064101.

25. Motter, A. E., Myers, S. A., Anghel, M. & Nishikawa, T. Spontaneous synchrony in power-grid networks. *Nat. Phys.* **9**, 191–197 (2013). https://doi.org/10.1038/nphys2535.

26. Dörfler, F. & Bullo, F. Synchronization in complex networks of phase oscillators: a survey. *Automatica* **50**, 1539–1564 (2014). https://doi.org/10.1016/j.automatica.2014.04.012.

27. Gross, T. & Blasius, B. Adaptive coevolutionary networks: a review. *J. R. Soc. Interface* **5**, 259–271 (2008). https://doi.org/10.1098/rsif.2007.1229.

28. Pope, M., Seguin, C., Varley, T. F., Faskowitz, J. & Sporns, O. Co-evolving dynamics and topology in a coupled oscillator model of resting brain function. *NeuroImage* **277**, 120266 (2023). https://doi.org/10.1016/j.neuroimage.2023.120266.

29. Bullmore, E. & Sporns, O. Complex brain networks: graph theoretical analysis of structural and functional systems. *Nat. Rev. Neurosci.* **10**, 186–198 (2009). https://doi.org/10.1038/nrn2575.

30. Bassett, D. S. & Sporns, O. Network neuroscience. *Nat. Neurosci.* **20**, 353–364 (2017). https://doi.org/10.1038/nn.4502.

31. Suárez, L. E., Markello, R. D., Betzel, R. F. & Mišić, B. Linking structure and function in macroscale brain networks. *Trends Cogn. Sci.* **24**, 302–315 (2020). https://doi.org/10.1016/j.tics.2020.01.008.

32. Buzsáki, G. & Draguhn, A. Neuronal oscillations in cortical networks. *Science* **304**, 1926–1929 (2004). https://doi.org/10.1126/science.1099745.

33. Fries, P. Rhythms for cognition: communication through coherence. *Neuron* **88**, 220–235 (2015). https://doi.org/10.1016/j.neuron.2015.09.034.

34. Breakspear, M., Heitmann, S. & Daffertshofer, A. Generative models of cortical oscillations: neurobiological implications of the Kuramoto model. *Front. Hum. Neurosci.* **4**, 190 (2010). https://doi.org/10.3389/fnhum.2010.00190.

35. Honey, C. J., Kötter, R., Breakspear, M. & Sporns, O. Network structure of cerebral cortex shapes functional connectivity on multiple time scales. *Proc. Natl Acad. Sci. USA* **104**, 10240–10245 (2007). https://doi.org/10.1073/pnas.0701519104.

36. Honey, C. J. et al. Predicting human resting-state functional connectivity from structural connectivity. *Proc. Natl Acad. Sci. USA* **106**, 2035–2040 (2009). https://doi.org/10.1073/pnas.0811168106.

37. Cabral, J., Hugues, E., Sporns, O. & Deco, G. Role of local network oscillations in resting-state functional connectivity. *NeuroImage* **57**, 130–139 (2011). https://doi.org/10.1016/j.neuroimage.2011.04.010.

38. Deco, G., Jirsa, V., McIntosh, A. R., Sporns, O. & Kötter, R. Key role of coupling, delay, and noise in resting brain fluctuations. *Proc. Natl Acad. Sci. USA* **106**, 10302–10307 (2009). https://doi.org/10.1073/pnas.0901831106.

39. Betzel, R. F., Fukushima, M., He, Y., Zuo, X.-N. & Sporns, O. Dynamic fluctuations coincide with periods of high and low modularity in resting-state functional brain networks. *NeuroImage* **127**, 287–297 (2016). https://doi.org/10.1016/j.neuroimage.2015.12.001.

40. Shine, J. M. et al. The dynamics of functional brain networks: integrated network states during cognitive task performance. *Neuron* **92**, 544–554 (2016). https://doi.org/10.1016/j.neuron.2016.09.018.

41. Jiang, L. et al. Gene transcription, neurotransmitter, and neurocognition signatures of brain structural-functional coupling variability. *Nat. Commun.* **16**, 7623 (2025). https://doi.org/10.1038/s41467-025-63000-5.

42. Zamani Esfahlani, F. et al. High-amplitude cofluctuations in cortical activity drive functional connectivity. *Proc. Natl Acad. Sci. USA* **117**, 28393–28401 (2020). https://doi.org/10.1073/pnas.2005531117.

43. Faskowitz, J., Zamani Esfahlani, F., Jo, Y., Sporns, O. & Betzel, R. F. Edge-centric functional network representations of human cerebral cortex reveal overlapping system-level architecture. *Nat. Neurosci.* **23**, 1644–1654 (2020). https://doi.org/10.1038/s41593-020-00719-y.

44. Novelli, L. & Razi, A. A mathematical perspective on edge-centric brain functional connectivity. *Nat. Commun.* **13**, 2693 (2022). https://doi.org/10.1038/s41467-022-29775-7.

45. Ott, E. & Antonsen, T. M. Low dimensional behavior of large systems of globally coupled oscillators. *Chaos* **18**, 037113 (2008). https://doi.org/10.1063/1.2930766.

46. Ott, E. & Antonsen, T. M. Long time evolution of phase oscillator systems. *Chaos* **19**, 023117 (2009). https://doi.org/10.1063/1.3136851.

47. Kowalczyk, M., Liò, P. & Struzik, Z. R. *Transfer dynamics and spectral cascades in graph-coupled Kuramoto networks* (arXiv, 2026). https://arxiv.org/abs/2609.28432.

48. Zabaleta-Ortega, Á., Masoller, C. & Guzmán-Vargas, L. Unveiling synchronization transitions in networks of coupled oscillators through persistent homology of local structures. *Sci. Rep.* **15**, 42772 (2025). https://doi.org/10.1038/s41598-025-27083-w.

49. Galindo-Leon, E. E., Nolte, G., Pieper, F., Engler, G. & Engel, A. K. Causal interactions between amplitude correlation and phase coupling in cortical networks. *Sci. Rep.* **15**, 11975 (2025). https://doi.org/10.1038/s41598-025-95306-1.

50. Risken, H. *The Fokker–Planck Equation: Methods of Solution and Applications* (Springer, 1989).

51. Gardiner, C. *Stochastic Methods: A Handbook for the Natural and Social Sciences* (Springer, 2009).

52. van Kampen, N. G. *Stochastic Processes in Physics and Chemistry* (Elsevier, 2007).

53. Kubo, R. The fluctuation-dissipation theorem. *Rep. Prog. Phys.* **29**, 255–284 (1966). https://doi.org/10.1088/0034-4885/29/1/306.

54. Zwanzig, R. Memory effects in irreversible thermodynamics. *Phys. Rev.* **124**, 983–992 (1961). https://doi.org/10.1103/PhysRev.124.983.

55. Mori, H. Transport, collective motion, and Brownian motion. *Prog. Theor. Phys.* **33**, 423–455 (1965). https://doi.org/10.1143/PTP.33.423.

56. Chorin, A. J., Hald, O. H. & Kupferman, R. Optimal prediction and the Mori–Zwanzig representation of irreversible processes. *Proc. Natl Acad. Sci. USA* **97**, 2968–2973 (2000). https://doi.org/10.1073/pnas.97.7.2968.

57. Mezić, I. Spectral properties of dynamical systems, model reduction and decompositions. *Nonlinear Dyn.* **41**, 309–325 (2005). https://doi.org/10.1007/s11071-005-2824-x.

58. Schmid, P. J. Dynamic mode decomposition of numerical and experimental data. *J. Fluid Mech.* **656**, 5–28 (2010). https://doi.org/10.1017/S0022112010001217.

59. Rowley, C. W., Mezić, I., Bagheri, S., Schlatter, P. & Henningson, D. S. Spectral analysis of nonlinear flows. *J. Fluid Mech.* **641**, 115–127 (2009). https://doi.org/10.1017/S0022112009992059.

60. Brunton, S. L., Proctor, J. L. & Kutz, J. N. Discovering governing equations from data by sparse identification of nonlinear dynamical systems. *Proc. Natl Acad. Sci. USA* **113**, 3932–3937 (2016). https://doi.org/10.1073/pnas.1517384113.

Acknowledgements

This research received no external funding or grant support.

Author contributions

Yousef Jamali is the sole author and is responsible for the conceptualization, study design, methodology, investigation, software and computational analysis, validation, interpretation of results, preparation and revision of the manuscript, and approval of the final version.

Competing interests

The author declares no competing financial or non-financial interests.

Ethics statement

Only synthetic oscillator-network simulations were performed; no participants, human samples or experimental animals were involved.

Figure legends

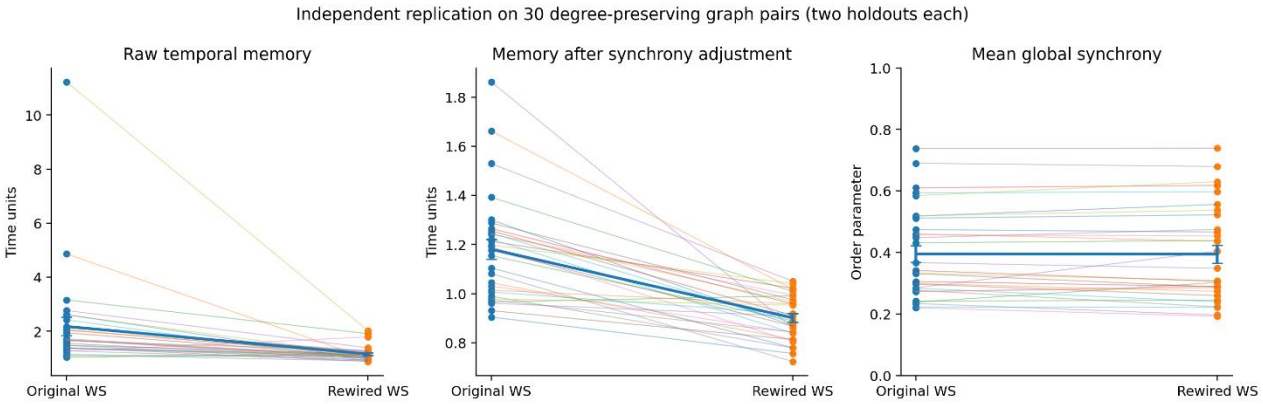
Figure 1 | Degree-preserving topology intervention uncovers different memory at similar average coherence. Results from 30 independent graph–frequency pairs with two holdout noise realizations each. The principal endpoint is the first-$1/e$ time of the centered autocorrelation of $q(t)$; secondary endpoints include the nonlinear/lagged synchrony-adjusted residual and the global order parameter $r(t)$. Lines identify matched graph pairs and error summaries are across pairs. Coupling was tuned on separate training paths only.

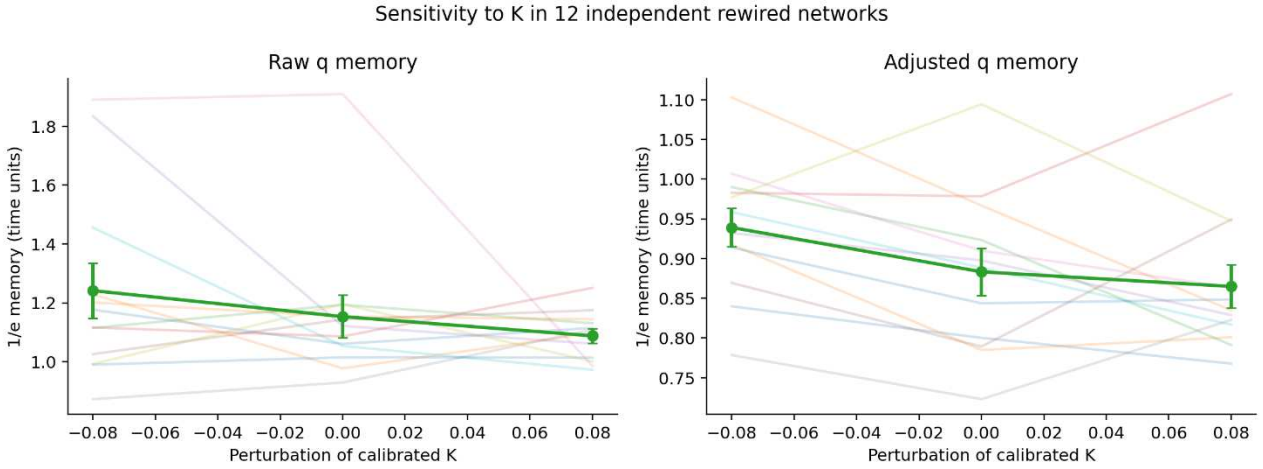
Figure 2 | Sensitivity of memory contrasts to coupling calibration. Tests in 12 graph pairs at the calibrated rewired coupling and a perturbation of ± 0.08, with separately generated noise. The panel is a robustness study, not another independent primary cohort.

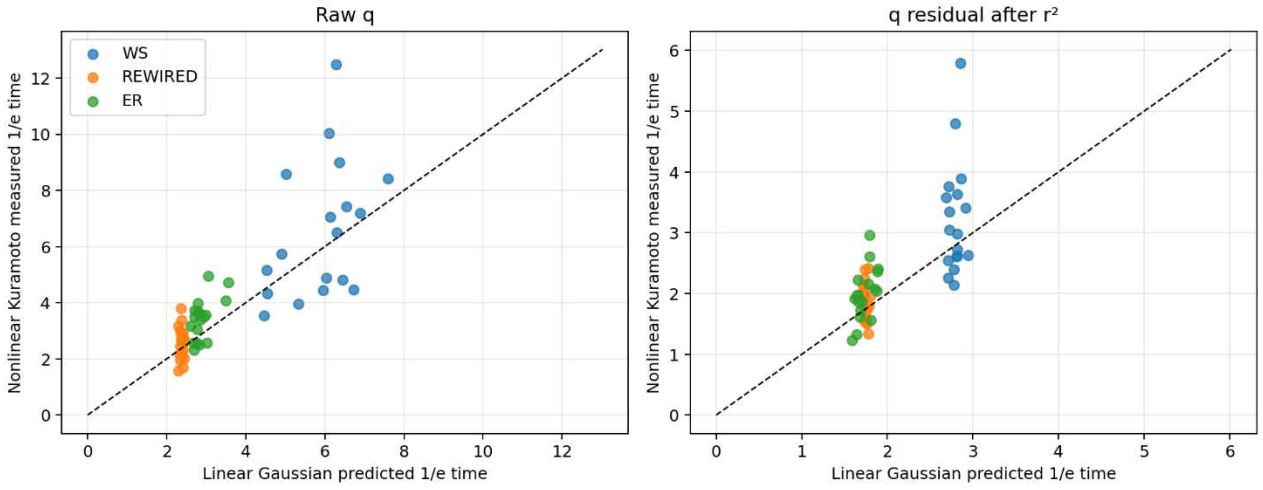
Figure 3 | Near-locking spectral theory compared with nonlinear simulation. The predicted first-crossing memory times of the phase-coherence contrast are compared with those measured in nonlinear simulations of original small-world, degree-preserving rewired and Erdős–Rényi networks. The left panel shows the raw contrast and the right panel shows the residual after adjustment for the global order measure used in the original Stage 4 analysis. The approximation assumes small transverse fluctuations around locking. Supplementary Fig. S3 separately displays how structural spectral quantities relate to the predicted memory time.

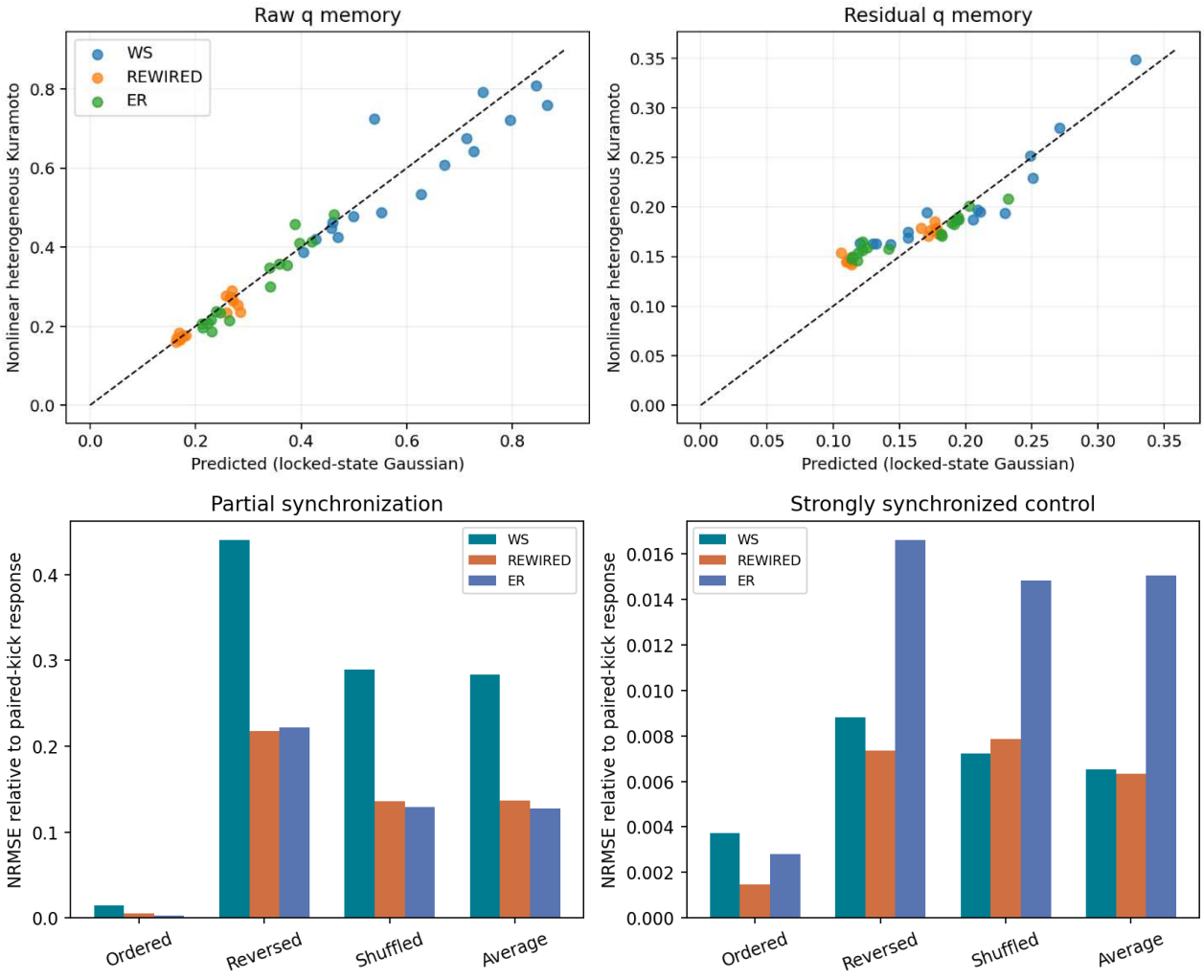
Figure 4 | Heterogeneous locked-state extension. Measured versus theory-predicted first-$1/e$ times for 48 stable heterogeneously locked systems, including the contribution of the observable's linear and quadratic mode projections. The reported Pearson correlation is 0.975.

Figure 5 | Temporal ordering of tangent dynamics under partial synchrony. Comparison of small-kick response reconstruction from the true time-ordered Jacobian sequence and ablated sequences (reversed, shuffled or averaged). The response concerns kicked-versus-reference trajectories with common noise, not the spontaneous autocorrelation of q.


Independent replication on 30 degree-preserving graph pairs (two holdouts each)
Raw temporal memory
Time units
Original WS
Rewired WS
Memory after synchrony adjustment
Time units
Original WS
Rewired WS
Mean global synchrony
Order parameter
Original WS
Rewired WS


Sensitivity to K in 12 independent rewired networks
Raw q memory
1/e memory (time units)
Perturbation of calibrated K
Adjusted q memory
1/e memory (time units)
Perturbation of calibrated K


Raw q
WS
REWIRED
ER
Nonlinear Kuramoto measured 1/e time
Linear Gaussian predicted 1/e time
q residual after r²
Nonlinear Kuramoto measured 1/e time
Linear Gaussian predicted 1/e time


Raw q memory
WS
REWIRED
ER
Nonlinear heterogeneous Kuramoto
Predicted (locked-state Gaussian)
Residual q memory
Nonlinear heterogeneous Kuramoto
Predicted (locked-state Gaussian)
Partial synchronization
WS
REWIRED
ER
NRMSE relative to paired-kick response
Ordered
Reversed
Shuffled
Average
Strongly synchronized control
WS
REWIRED
ER
NRMSE relative to paired-kick response
Ordered
Reversed
Shuffled
Average

Supplementary Files

This is a list of supplementary files associated with this preprint. Click to download.

- SupplementaryInformation.pdf
- ReproducibilityMaterials.zip